Science Advances

AAAS

advances.sciencemag.org/cgi/content/full/3/12/eaaq0208/DC1

Supplementary Materials for

Aggregation-induced emission in lamellar solids of colloidal perovskite quantum wells

Jakub Jagielski, Sudhir Kumar, Mingchao Wang, Declan Scullion, Robert Lawrence, Yen-Ting Li, Sergii Yakunin, Tian Tian, Maksym V. Kovalenko, Yu-Cheng Chiu, Elton J. G. Santos, Shangchao Lin, Chih-Jen Shih

Published 22 December 2017, *Sci. Adv.* **3**, eaaq0208 (2017)
DOI: 10.1126/sciadv.aaq0208

The PDF file includes:

- fig. S18. Observation of ASE.
- fig. S19. The threshold behavior for the intensity of the ASE band.
- table S1. Ligand volumes.
- table S2. Absolute η_{PL} summary.
- Legends for movies S1 to S3
- References (*65–68*)

Other Supplementary Material for this manuscript includes the following:
(available at advances.sciencemag.org/cgi/content/full/3/12/eaaq0208/DC1)

- movie S1 (.mp4 format). Ab initio MD of the $n = 1$ geometry viewed along the 001 axis.
- movie S2 (.mp4 format). Ab initio MD of the $n = 1$ geometry viewed along the 100 axis.
- movie S3 (.mp4 format). Ab initio MD of the $n = 1$ geometry viewed along the 010 axis.

Supplementary Text

text S1. Blue DC LEDs.

Considering the record high solid state η_{PL} of trilayer (n = 3) $MAPbBr_3$ perovskites, we also investigated their role as a monochromatic pure-blue phosphor in the DC-LEDs. Blue DC-LEDs were fabricated by using n = 3 MA CQWs as phosphor. The blue DC-LED exhibits a η_{LEmax} of 5.1 lm W^{-1} with a peak emission at 468 nm and a narrow FWHM of 21±1 nm (fig. S16). The device also demonstrates excellent color-saturation with $CIE_{x,y}$ coordinates of (0.140, 0.150) (fig. S13). The high efficiency blue perovskite DC-LED shows over 85% coverage of Rec. 2020 color gamut in the 1931 CIE color space by substituting the blue counterpart from the gamut. To the best of our knowledge, this is highest η_{LE} and a highest L_{max} = 15180 cd m^{-2} ever achieved in the quantum confined assemblies, such as perovskites and quantum dots. To the best of our knowledge, the pure blue emission chromaticity, have never been achieved based on any nanomaterial assemblies by far, through a monochromatic DC-LEDs (*65*).

text S2. ASE experiments.

Extremely high values of PLQYs and close stacking of perovskite CQWs, which leads into exciton delocalization, bring to easy realization of optical gain using bi-excitonic effects. This is proven by demonstration of amplified spontaneous emission (ASE) spectra, obtained upon pulsed excitation (400 nm, 100 fs) (fig. S18). There, the redshift of the ASE band can be associated with the bi-excitonic nature of the optical gain (*66*) which is enabled by effective exciton dynamics in drop-casted film. The pump intensity threshold for ASE is about 12 μJ cm^{-2} (fig. S19), one of the lowest among colloidal NCs emitting in the green range (*66–68*).

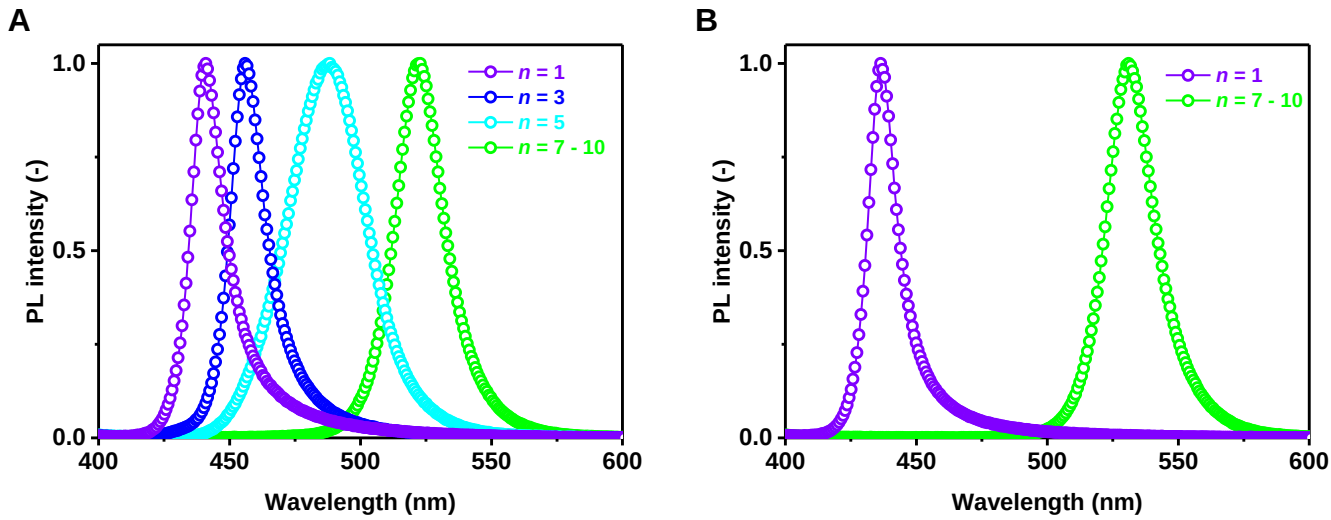

fig. S1. Photoluminescence properties of perovskite CQWs in solution. PL spectra under 370 nm excitation for colloidal solutions of (**A**) $MAPbBr_3$ and (**B**) $FAPbBr_3$ 2D perovskites as a function of layer number *n*.

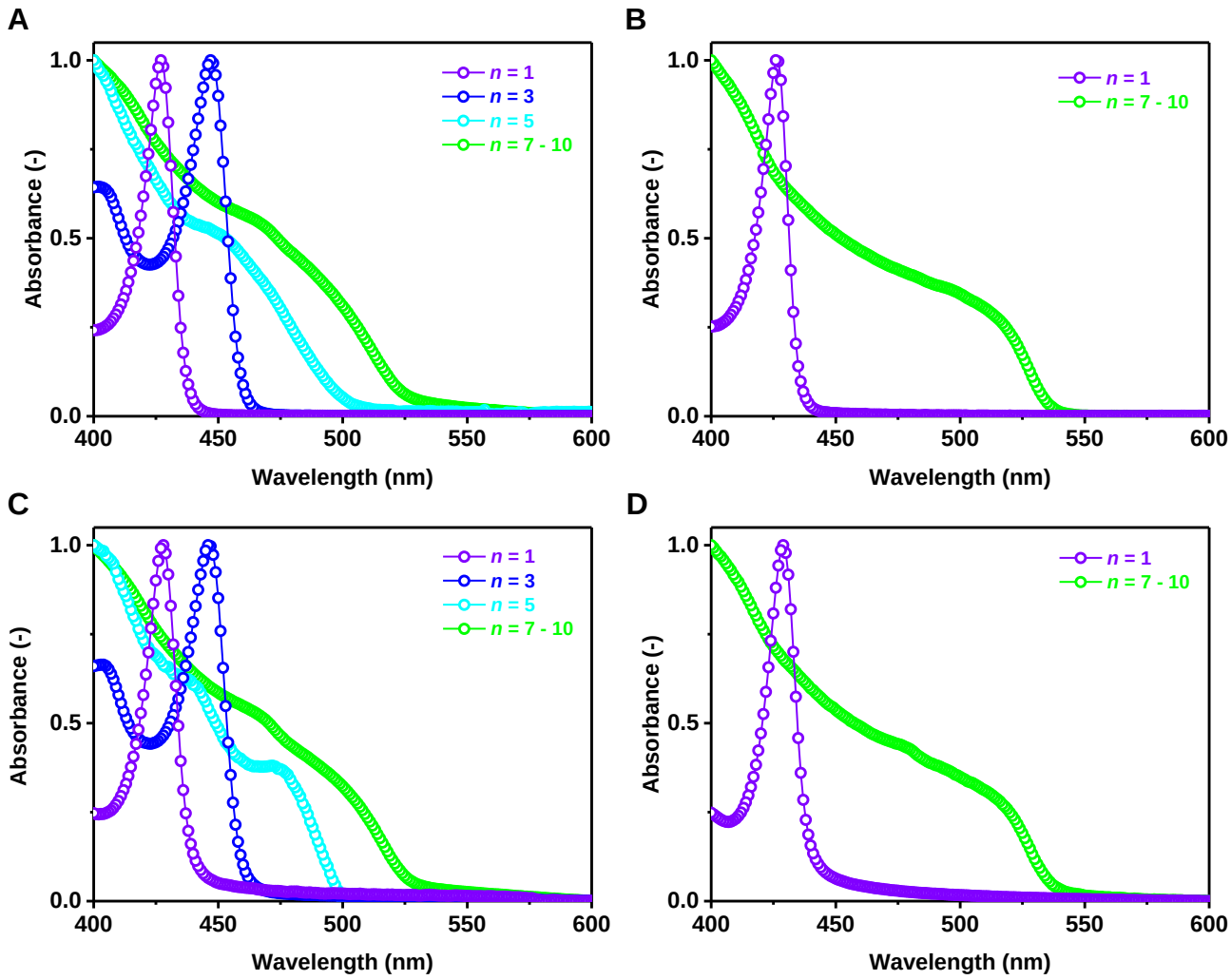

fig. S2. Optical absorption of perovskite CQW samples. UV-Vis absorption spectra determined for colloidal solutions of (**A**) $MAPbBr_3$ and (**B**) $FAPbBr_3$ 2D perovskites as a function of layer number *n*. Analogously, same measurements were conducted for MA- (**C**) and FA- (**D**) solid state counterparts. Only minor changes can be noticed between spectra taken for different states.

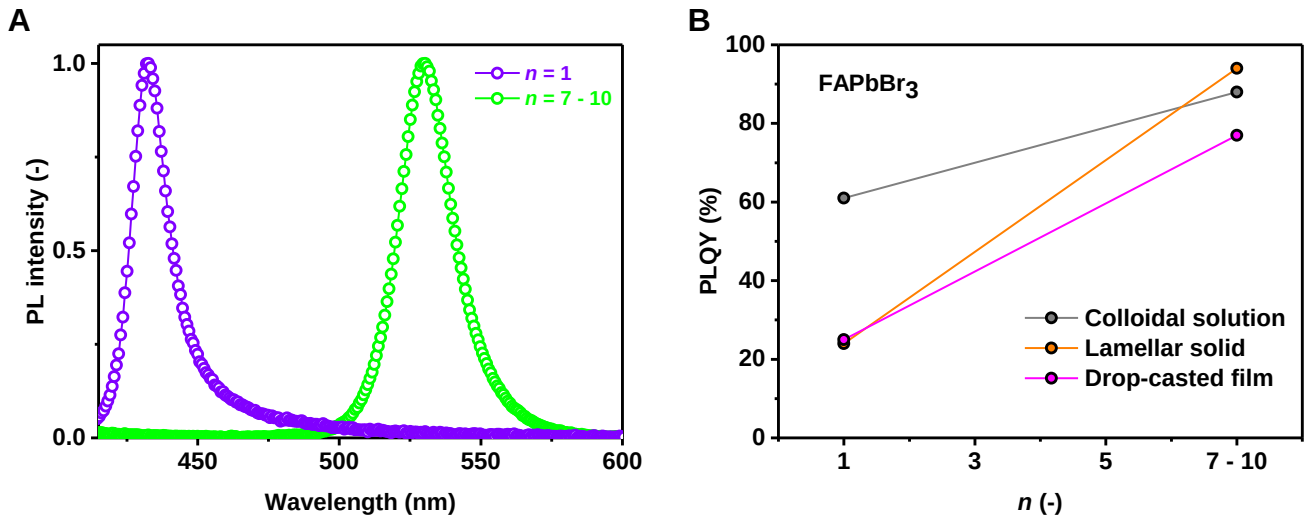

fig. S3. Photoluminescence properties of $FAPbBr_3$ CQWs. (**A**) Steady-state PL spectra of *n* = 1 and *n* = 7 – 10 FA lamellar solids. (**B**) Absolute PLQY for all three forms of CQWs – colloidal solution, lamellar solid and drop-casted film, as a function of layer number *n*.

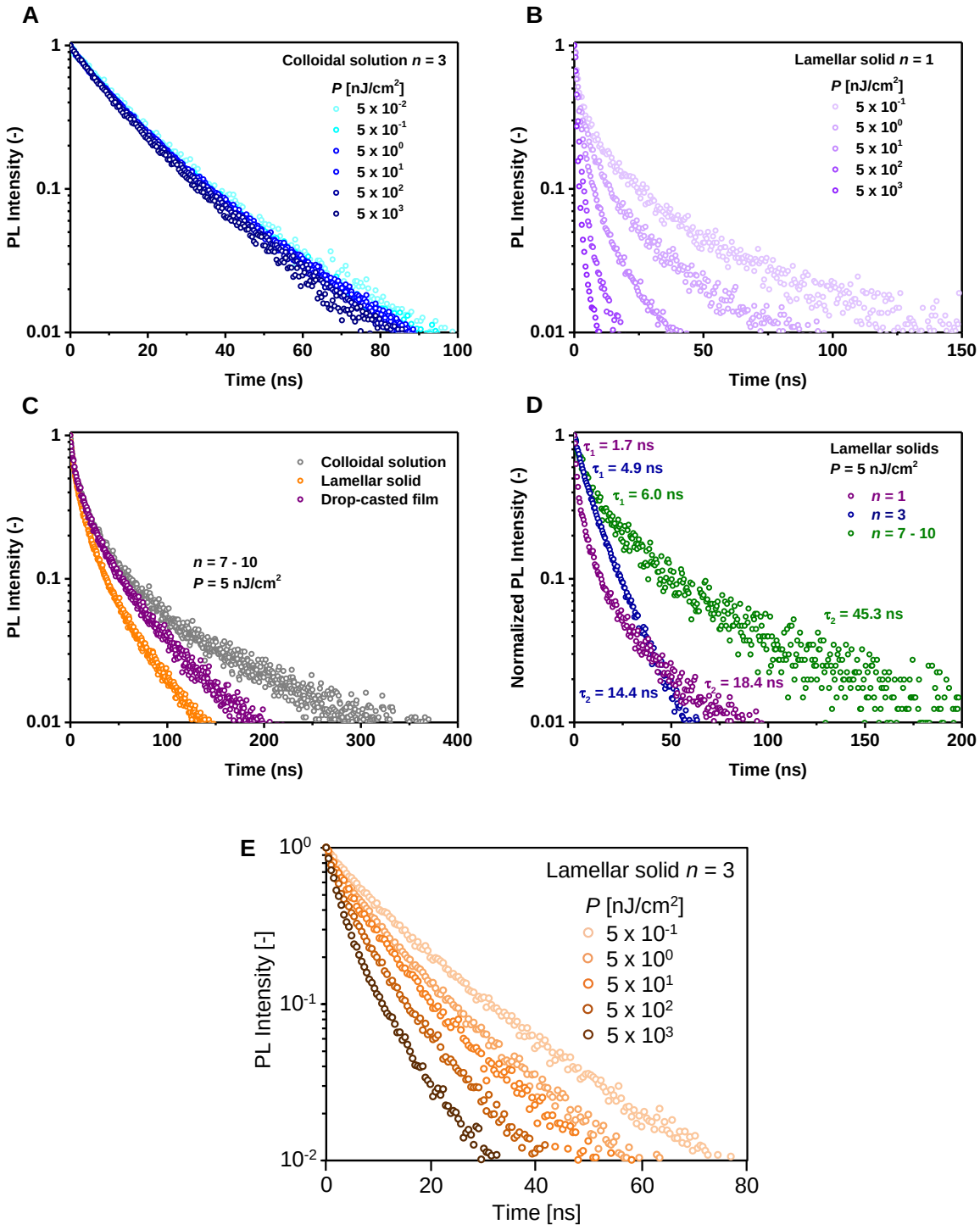
A
Colloidal solution n = 3
P [nJ/cm²]
5 x 10⁻²
5 x 10⁻¹
5 x 10⁰
5 x 10¹
5 x 10²
5 x 10³
PL Intensity (-)
Time (ns)
B
Lamellar solid n = 1
P [nJ/cm²]
5 x 10⁻¹
5 x 10⁰
5 x 10¹
5 x 10²
5 x 10³
PL Intensity (-)
Time (ns)
C
Colloidal solution
Lamellar solid
Drop-casted film
n = 7 - 10
P = 5 nJ/cm²
PL Intensity (-)
Time (ns)
D
Lamellar solids
P = 5 nJ/cm²
n = 1
n = 3
n = 7 - 10
τ1 = 1.7 ns
τ1 = 4.9 ns
τ1 = 6.0 ns
τ2 = 45.3 ns
τ2 = 18.4 ns
τ2 = 14.4 ns
Normalized PL Intensity (-)
Time (ns)
E
Lamellar solid n = 3
P [nJ/cm²]
5 x 10⁻¹
5 x 10⁰
5 x 10¹
5 x 10²
5 x 10³
PL Intensity [-]
Time [ns]

fig. S4. TRPL analysis of $MAPbBr_3$ perovskite CQWs. PL traces were recorded for (**A**) n = 3 colloidal solution and for (**B**) n = 1 lamellar solid at different pumping energies P. The former exhibits practically constant PL lifetime τ_e of ~20 ns over the whole intensity range, thus proving a lack of aggregation phenomena between individual CQWs. In case of n = 1 lamellar solid, biexponential decay curve can be observed and the lifetime τ_e gradually decreases from 25 to 6 ns as the pumping energy is increased. This particular exciton recombination behavior can be caused by formation of inter-particle aggregates, in which multiexciton recombination is more likely to take place. As a consequence, the excitons tend to follow the non-radiative path, which in turn decreases PLQY significantly. Panel (**C**) depicts comparison of PL traces measured at moderate P of 5 nJ/cm^2 for n = 7 – 10 MA sample in all three forms. (**D**) PL decay characteristics of lamellar solids based on n = 1, 3 and 7 – 10 at pumping energy of P = 5 nJ/cm^2 were compared. Clearly, the decrease of layer number n results in shorter lifetimes, which is an indication of strong quantum confinement effects in thin perovskite CQWs. (**E**) TRPL of n = 3 MA lamellar solid under various pumping energies.

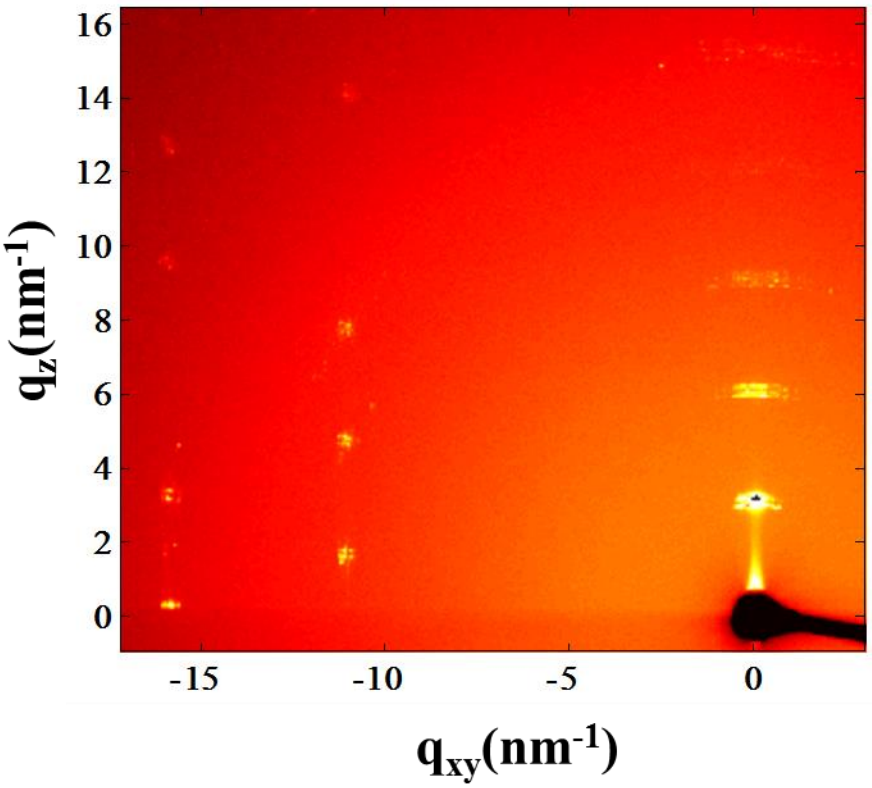

fig. S5. Synchrotron GIWAXS pattern of lamellar solid composed of *n* = 1 $MAPbBr_3$ CQWs. A sequence of superlattice diffraction signals starting at q_z = 2.96 nm^{-1} can be recognized. Therefore, the *d*-spacing is derived to be 2.1 nm. Subtraction of the ligand chain length (~0.9 nm) indicates CQW thickness of 1.2 nm.

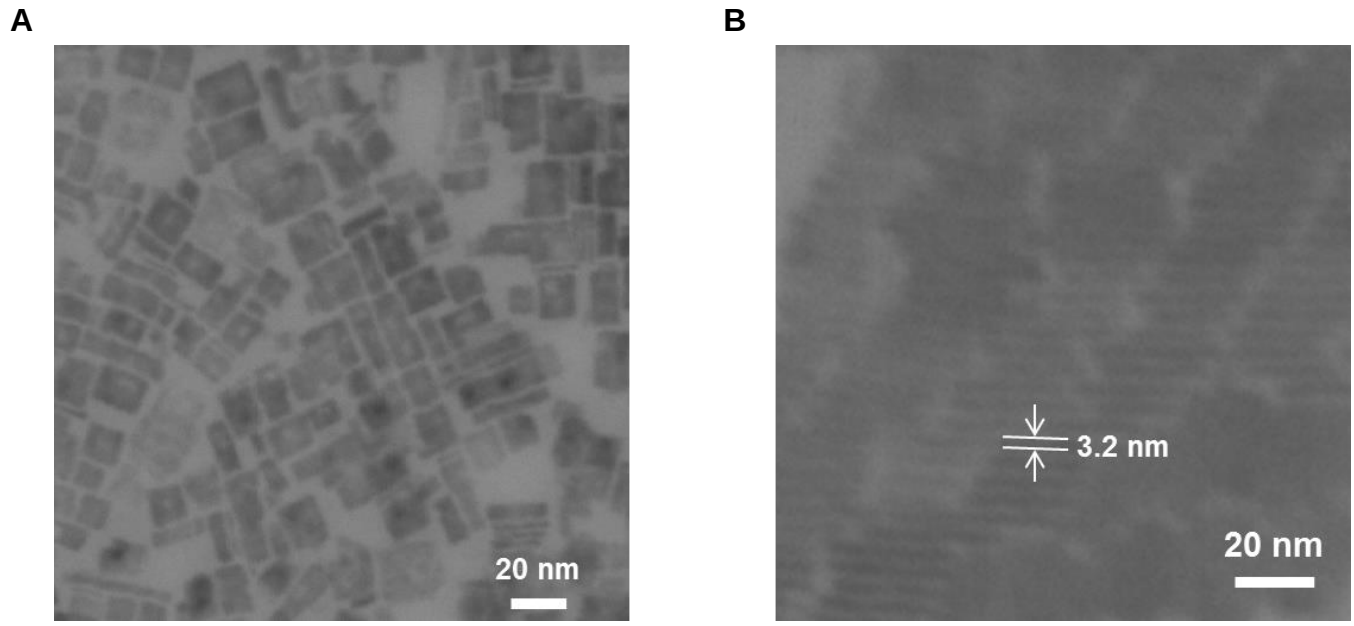

fig. S6. Morphology analysis of perovskite CQWs by means of STEM. (**A**) Micrograph showing nanostructures in n = 7 – 10 MA sample. Thick nanoplatelets (NPLs) aligning in "face-on" and standing orientations with lateral sizes of approximately 20 nm and thickness oscillating around 5 nm are visible on the TEM grid. (**B**) In case of n = 3 MA sample a group of stacked NPLs in standing orientation can be noticed. The interlayer spacing of 3.2 nm is determined, a result that coincides with the one obtained from GIWAXS.

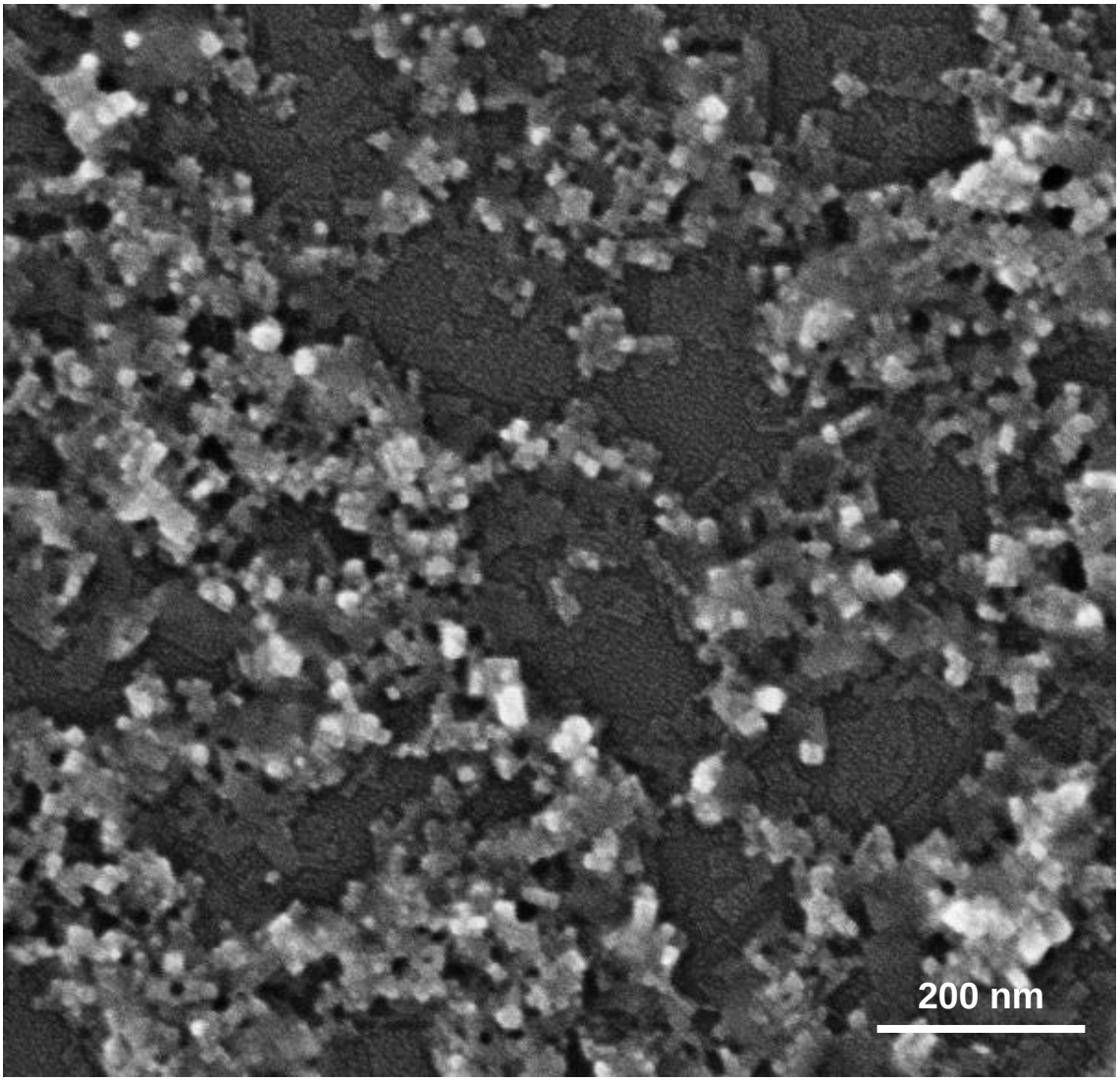

fig. S7. SEM analysis of the film morphology. The image reveals platelet-like nano-sized objects with preferred “face-on” orientation in the n = 7 – 10 MA lamellar solid.

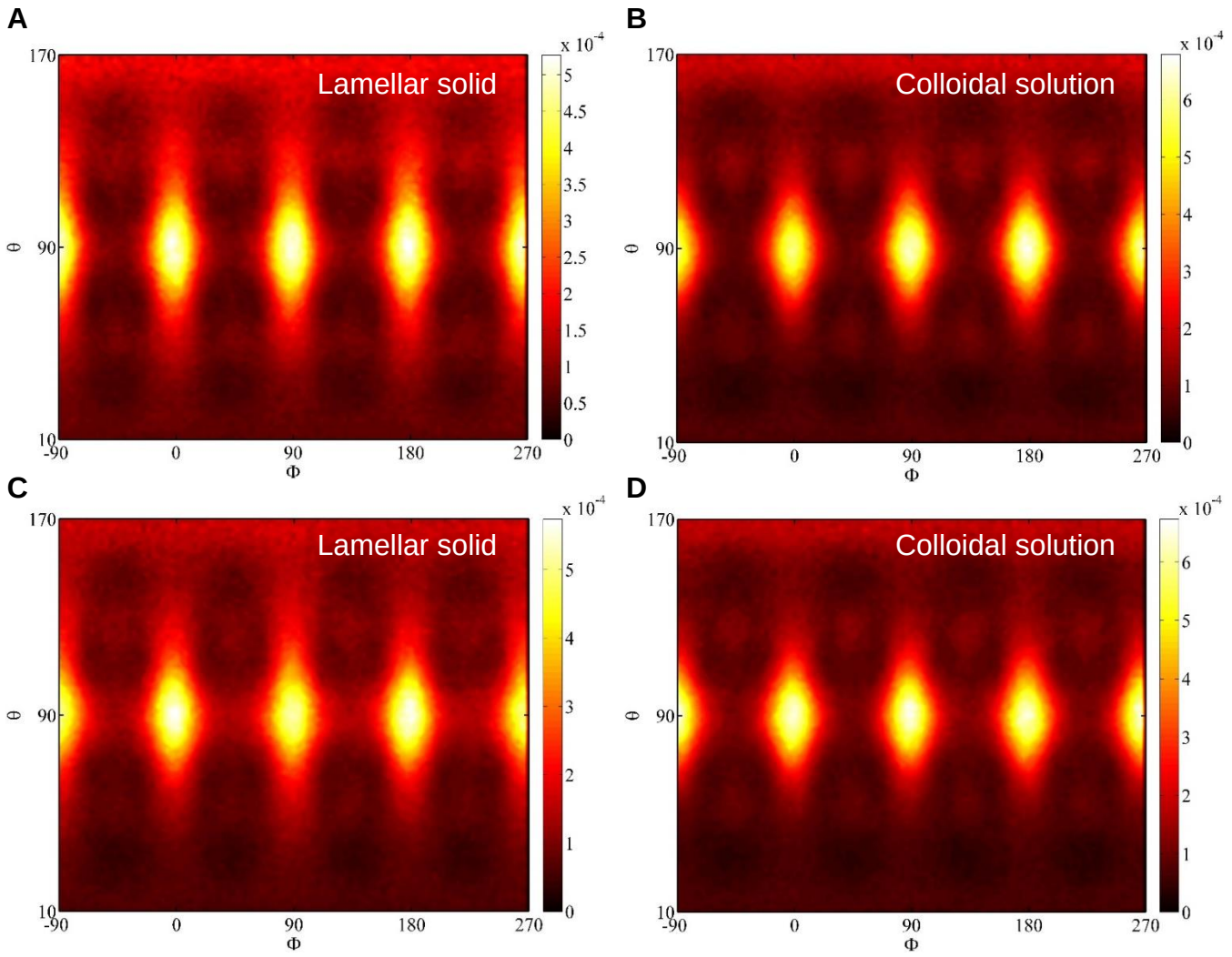

fig. S8. The orientation distribution map of bulk MA cations in *n* = 3 CQW. MD-calculated probability densities as a function of θ and ϕ for MA cations in the bulk of CQW with different surroundings. (**A**) Lamellar solid with 50% ligand surface coverage, (**B**) colloidal solution with 50% ligand surface coverage, (**C**) lamellar solid with 75% ligand surface coverage and (**D**) colloidal solution with 75% ligand surface coverage.

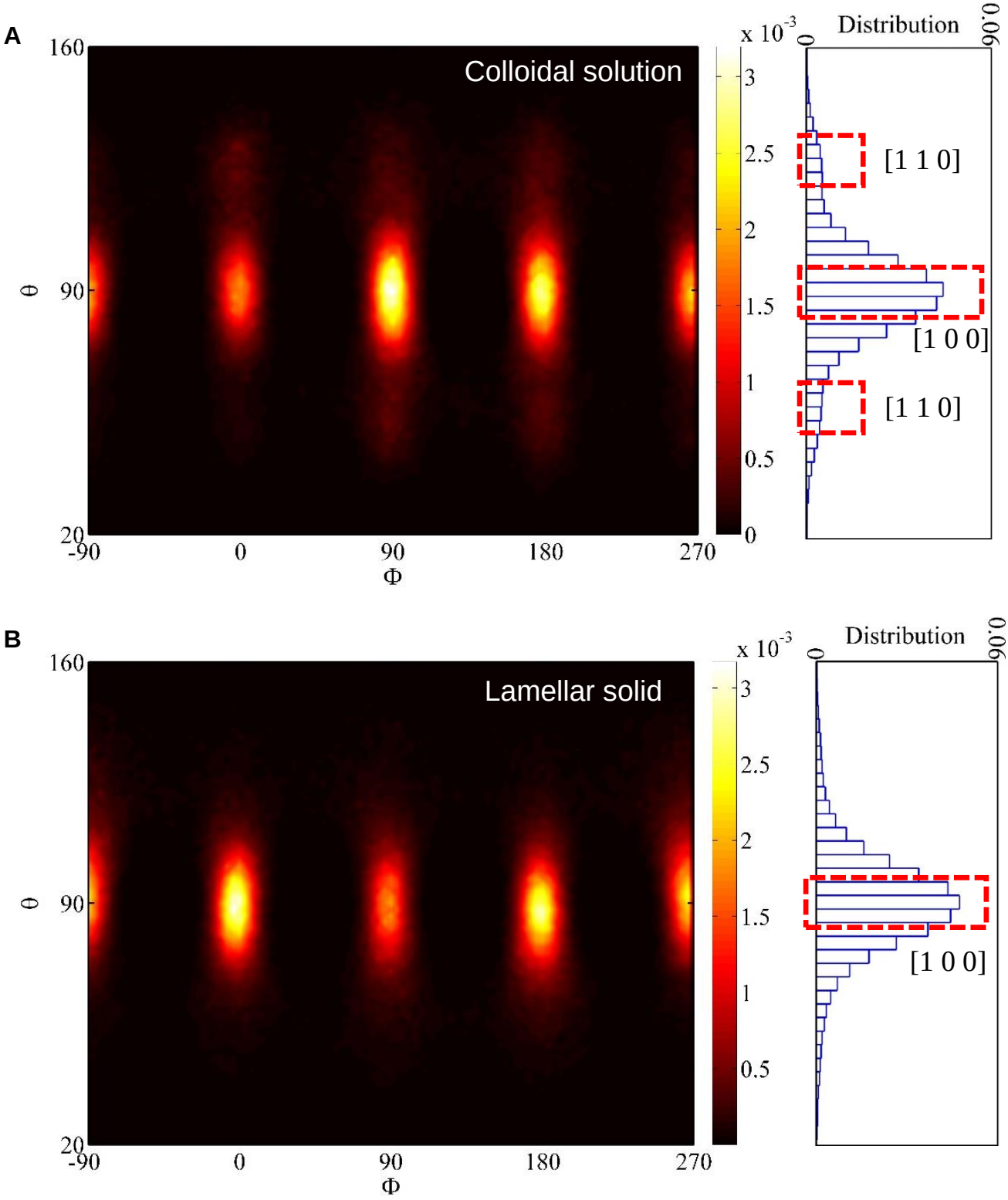
A
Colloidal solution
160
90
20
θ
-90
0
90
180
270
Φ
x 10^-3
3
2.5
2
1.5
1
0.5
0
Distribution
0
0.06
[1 1 0]
[1 0 0]
[1 1 0]
B
Lamellar solid
160
90
20
θ
-90
0
90
180
270
Φ
x 10^-3
3
2.5
2
1.5
1
0.5
Distribution
0
0.06
[1 0 0]

fig. S9. Surface MA cation orientation with 75% ligand coverage. Orientational distribution contour maps of surface MA cations as a function of θ and ϕ in (**A**) toluene solution and (**B**) lamellar solid. Right side of the panel depicts a probability histogram of the orientational distribution.

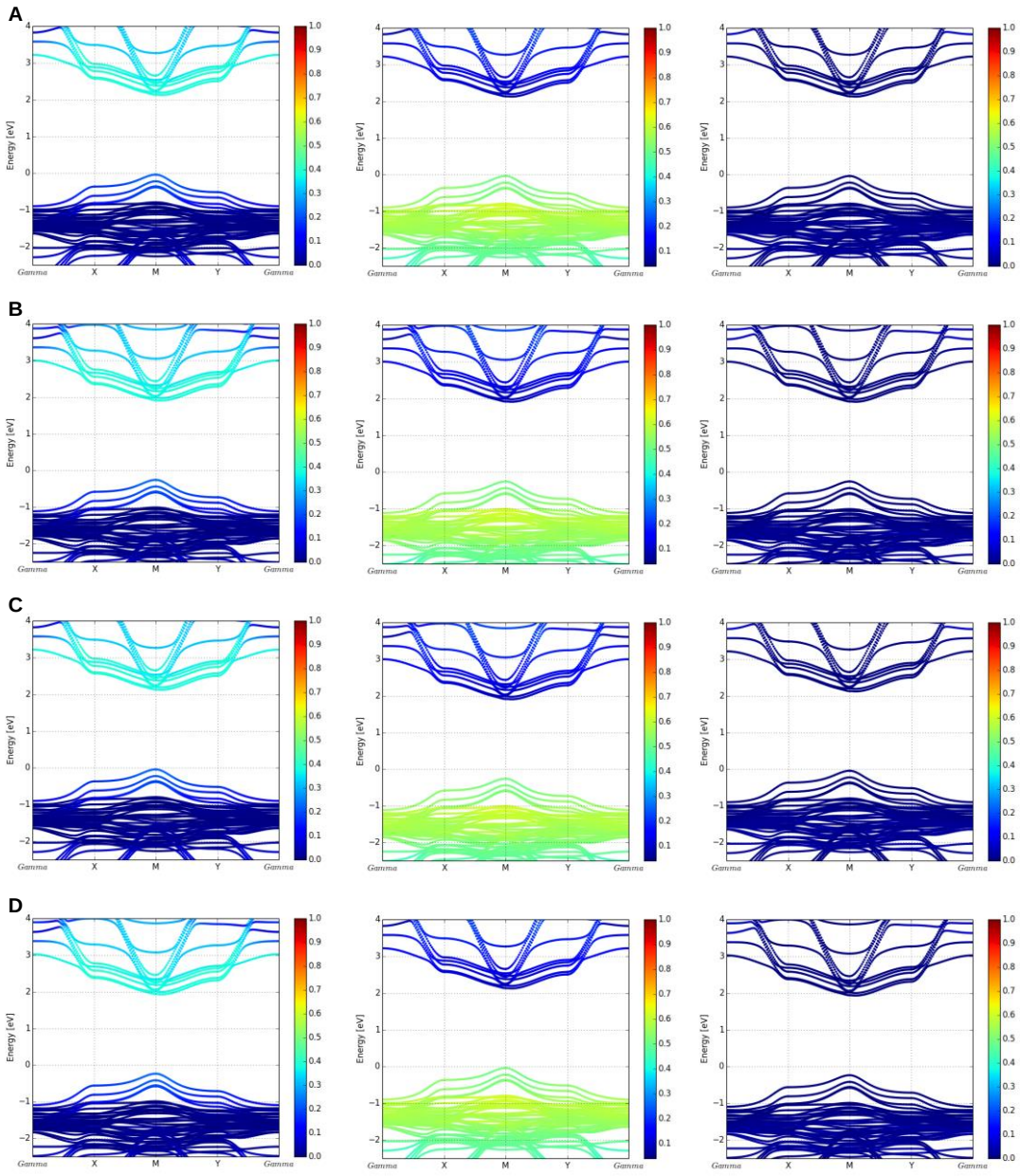
A
B
C
D
Energy [eV]
Gamma
X
M
Y

fig. S10. Electronic band structures projected on states of Pb atoms (left column), Br atoms (middle column), and CH_3NH_3 molecules (right column). Surface CH_3NH_3 cations are in the (**A**) [010], (**B**) [100], (**C**) [011] and (**D**) [111] configurations. The Fermi level has been set to zero in all panels. The gradient color bar indicates the contribution of the atoms to the band states. Pb atoms contribute mainly to the conduction bands whereas Br atoms have their majority contribution to the valence states. There is also a small contribution to the top of the valence band from the Pb atoms. CH_3NH_3 cations have very little contribution to the states around the Fermi level, which are further up or down in energy.

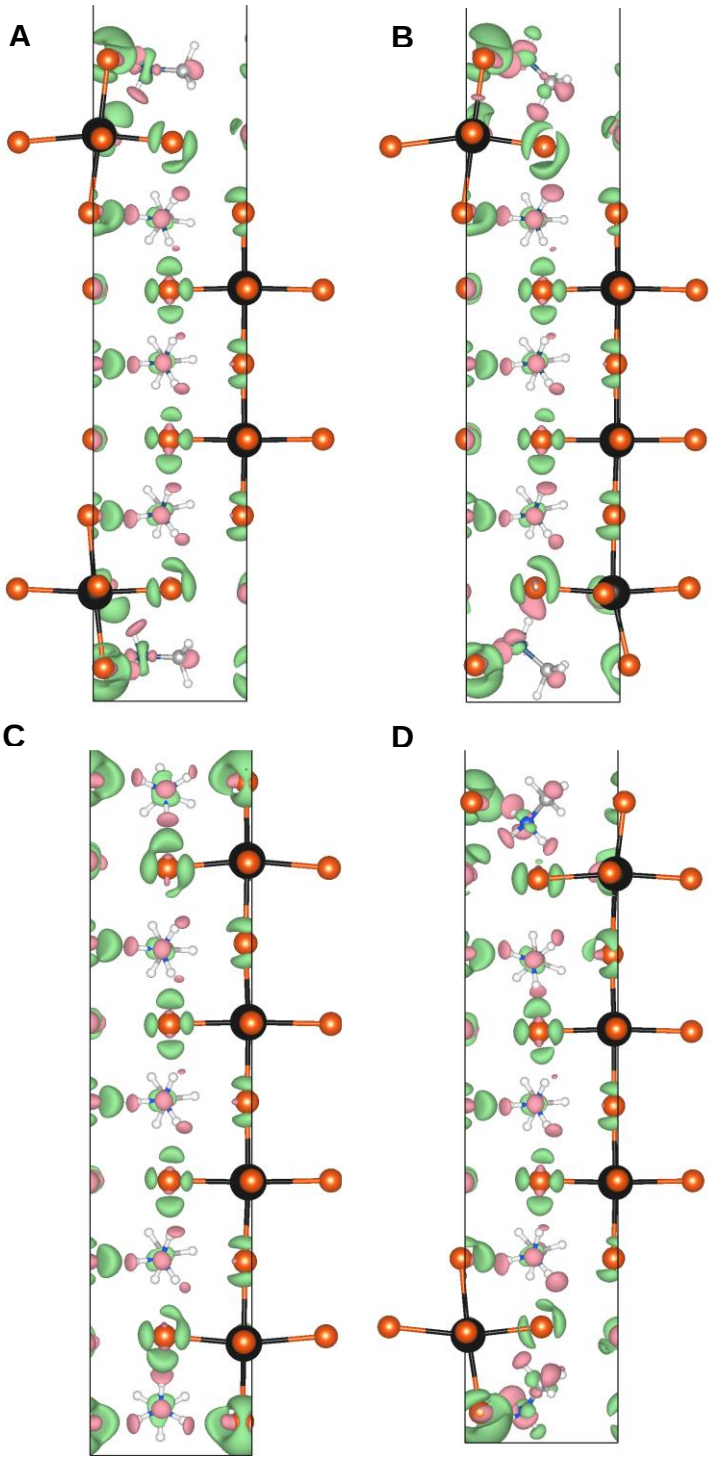
A
B
C
D

fig. S11. Charge density difference plots with different configurations. Charge density difference ($\Delta\rho = \rho[CH_3NH_3PbBr_3] - \rho[PbBr_3] - \rho[CH_3NH_3]$) of the four geometries with surface cations along: (a) [010], (b) [100], (c) [011] and (d) [111] configurations. Lead is black, bromine orange, nitrogen blue, carbon silver, hydrogen white. Positive (negative) charge is shown in green (pink). An isosurface value is set at $\pm$0.0021 e/Borh^3. Bulk CH_3NH_3 cations (inside of the layers) are in the [100] orientation for all configurations. Several geometrical distortions are observed in the lattice with a negative charge concentration towards the $PbBr_3^-$ cage.

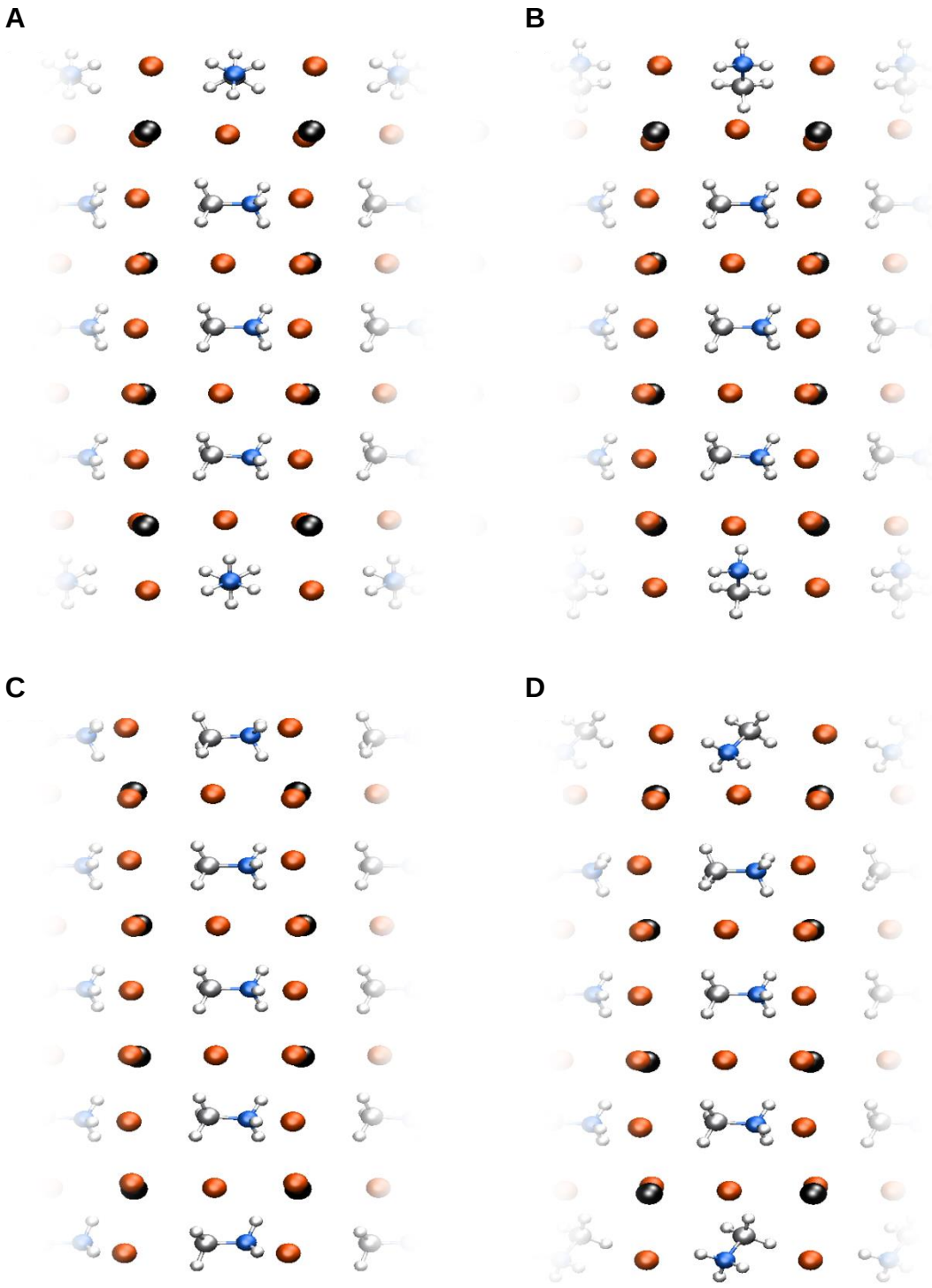

fig. S12. Final geometries after relaxation. Bulk $CH_3NH_3^+$ cations are in the 100 orientation for all configurations. (**A**) Surface cations in the 010 configuration. (**B**) 100 configuration. (**C**) 011 configuration. (**D**) 111 configuration.

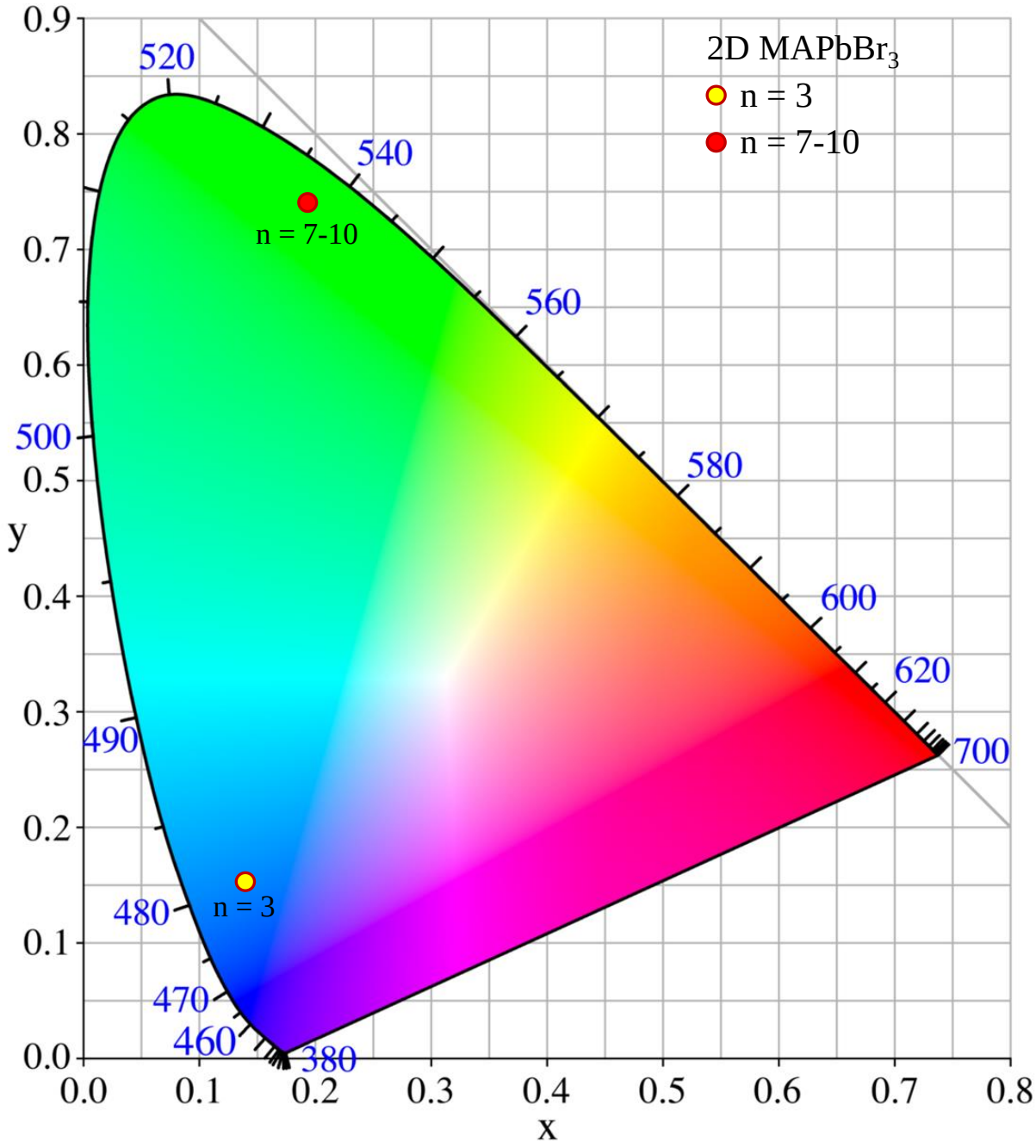

fig. S13. CIE chromaticity coordinates of green (*n* = 7 to 10) and blue (*n* = 3) CQW solid phosphor-based DC-LEDs.

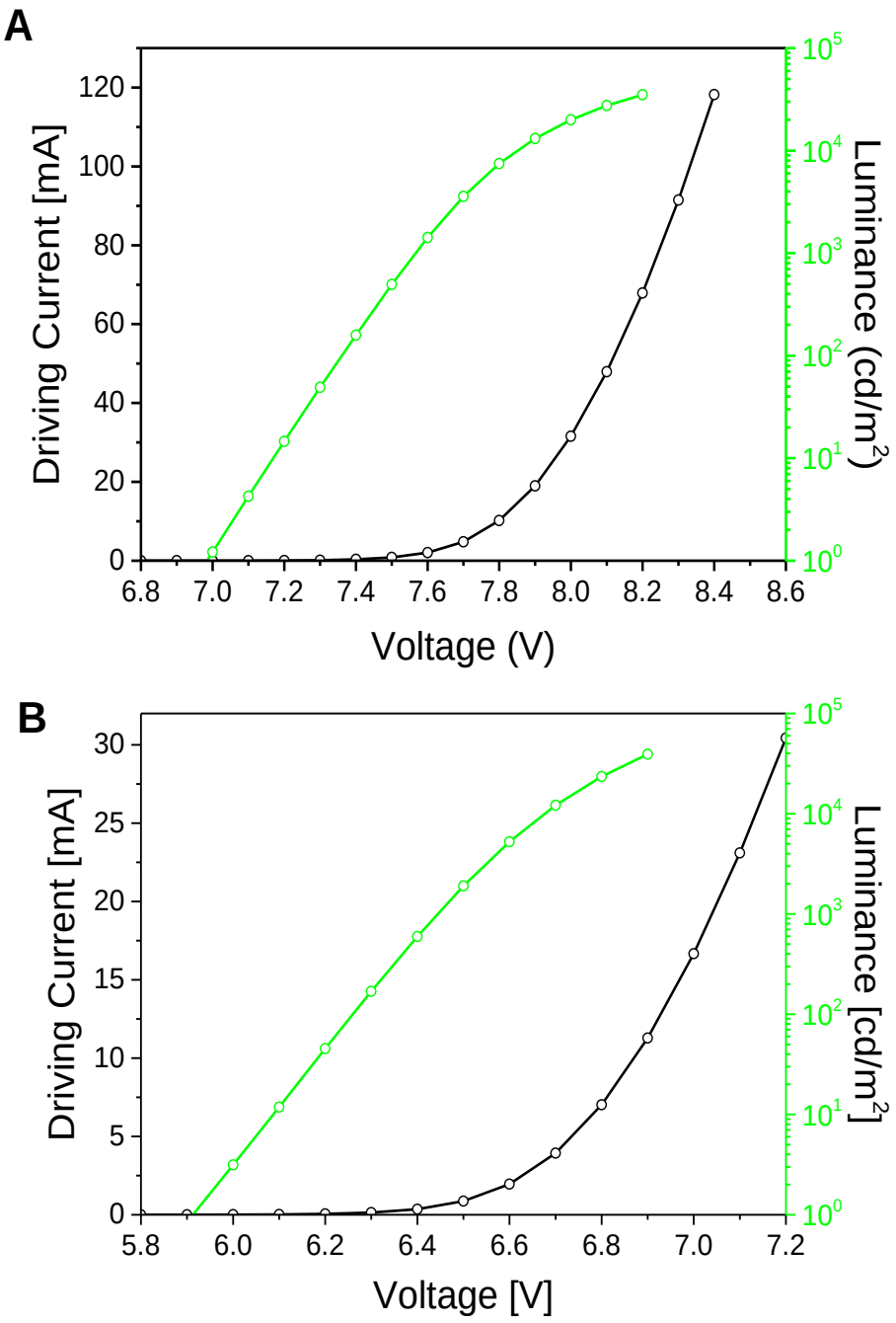

fig. S14. Driving current (*I*) and luminance (*L*) as a function of voltage (*V*). (**A**) Green DC-LED using n = 7 – 10 $MAPbBr_3$ CQW solid and (**B**) commercial green InGaN LED.

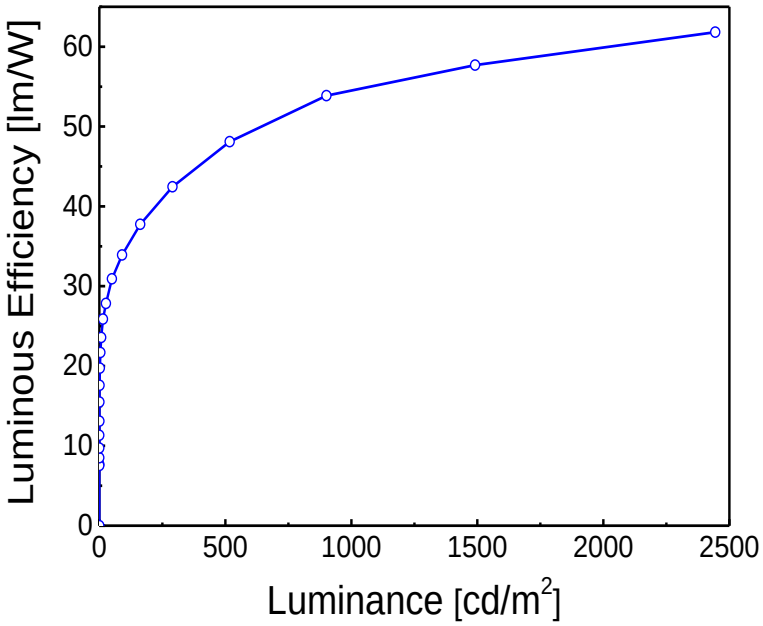

fig. S15. Luminous efficacy as a function of luminance for commercial blue GaN LED as pumping source.

A

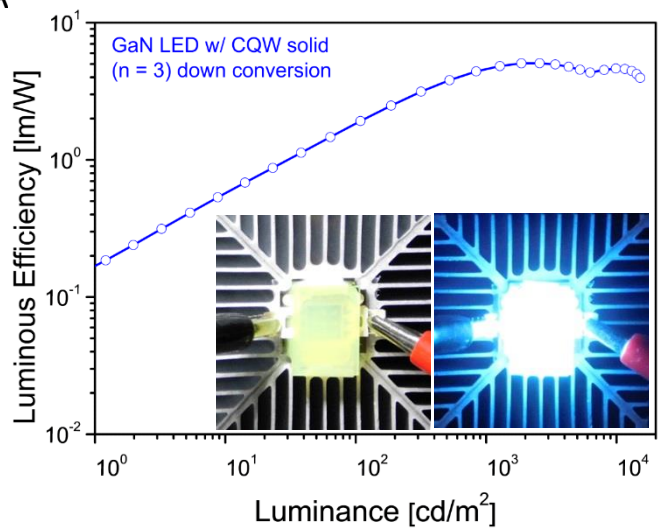
GaN LED w/ CQW solid
(n = 3) down conversion
Luminous Efficiency [lm/W]
Luminance [cd/m2]

B

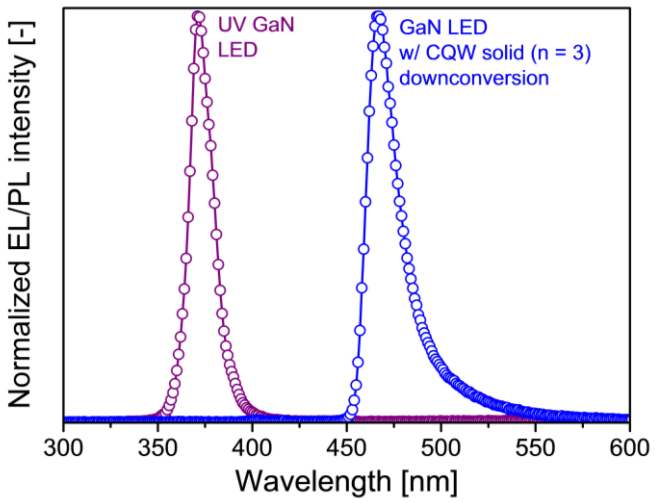
UV GaN
LED
GaN LED
w/ CQW solid (n = 3)
downconversion
Normalized EL/PL intensity [-]
Wavelength [nm]

C

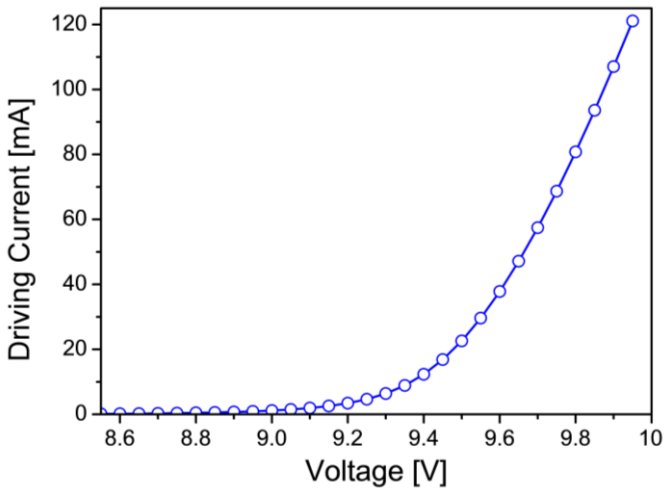
Driving Current [mA]
Voltage [V]

fig. S16. Demonstration of blue DC emission using *n* = 3 MA CQW solid. (**A**) Luminous efficacy as a function of luminance, Inset: Photographs of non-glowing blue DC-LED (left) and glowing DC-LED (right). (**B**) EL spectrum of pumping UV-LED before (violet) and PL spectrum of blue DC-LED after (blue). (**C**) Driving current (*I*) and luminance (*L*) as a function of voltage.

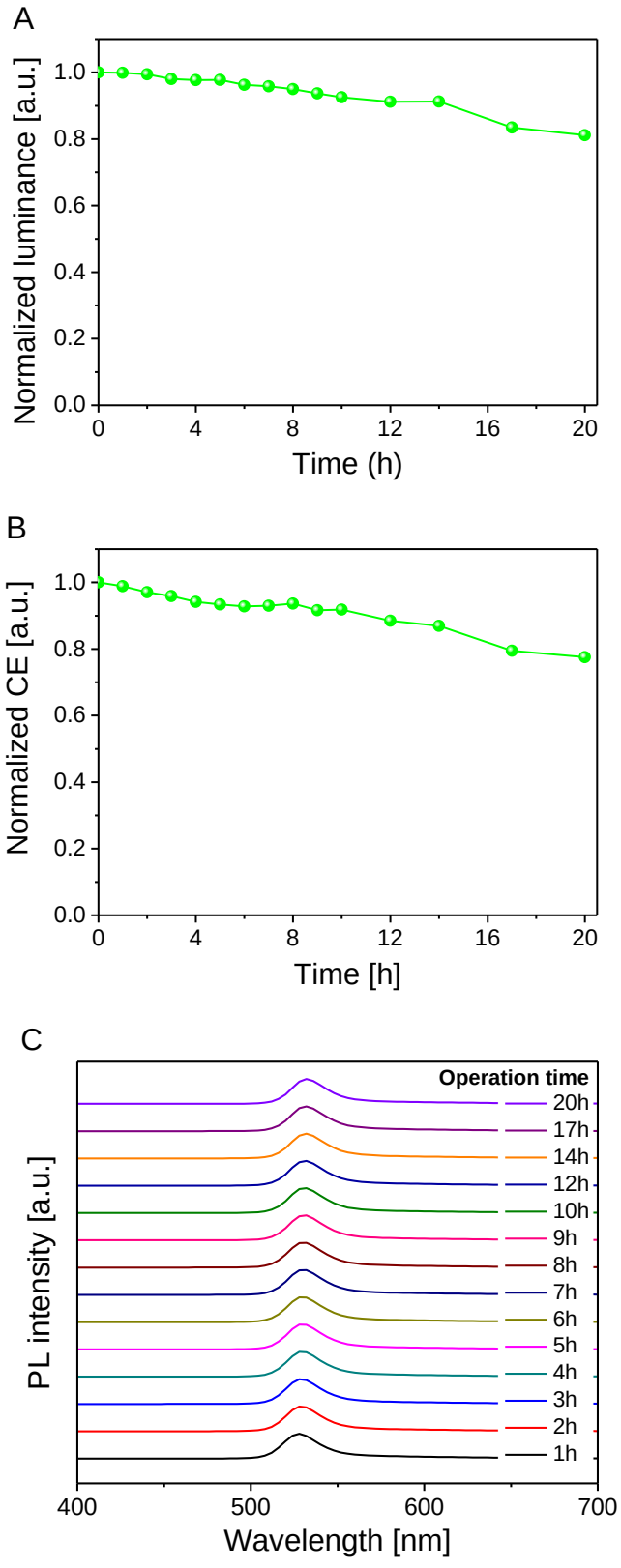
A
Normalized luminance [a.u.]
1.0
0.8
0.6
0.4
0.2
0.0
0
4
8
12
16
20
Time (h)
B
Normalized CE [a.u.]
1.0
0.8
0.6
0.4
0.2
0.0
0
4
8
12
16
20
Time [h]
C
PL intensity [a.u.]
Operation time
20h
17h
14h
12h
10h
9h
8h
7h
6h
5h
4h
3h
2h
1h
400
500
600
700
Wavelength [nm]

fig. S17. Operational stability of *n* = 7 to 10 MA CQW downconverting film. Normalized luminance (**A**) and luminous efficacy (η_{LE}) (**B**) as a function of operation time. (**C**) Photoluminescence (PL) emission spectra of green CQW dowconverting solid as a function of operation time.

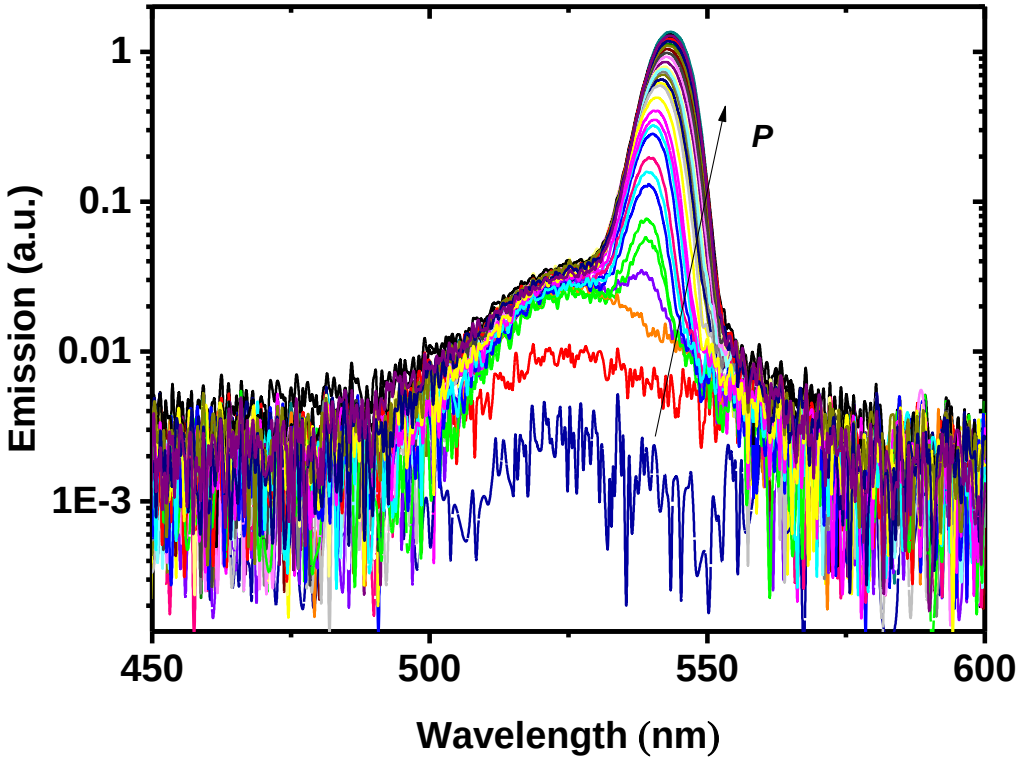

fig. S18. Observation of ASE. The plot shows ASE for films prepared from n = 7 – 10 MA perovskite CQWs by means of drop-casting, as a function of pumping energy density P.

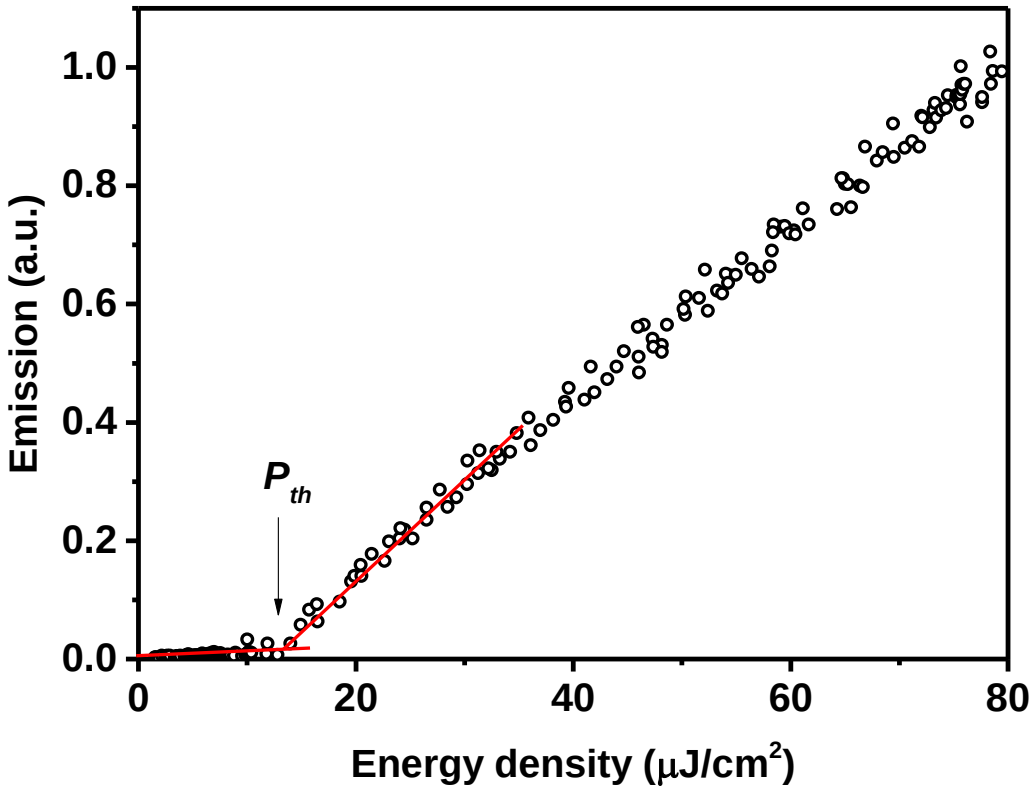

fig. S19. The threshold behavior for the intensity of the ASE band. Films prepared from *n* = 7 – 10 MA perovskite CQWs by means of drop-casting exhibit an energy density threshold of approximately 12 μJ/cm^2.

Supplementary Tables

table S1. Ligand volumes. Amounts of long-chain molecules added during the synthesis of various layered perovskite species.

Sample	OLA (mL)	OA (mL)	t-BuOH (mL)
***n* = 7-10**	0.625	0.025	10
***n* = 5**	1.25	0.025	10
***n* = 3**	1.875	0.250	-
***n* = 1**	6.250	0.500	-
***n* = 7-10 (FA)**	0.625	0.025	-
***n* = 1 (FA)**	6.250	0.500	-

table S2. Absolute η_{PL} summary. Exact values of absolute PLQY and their standard deviations for all synthesized perovskite CQWs in all three forms.

Sample	PLQY in colloidal solution (%)	PLQY in lamellar solid (%)	PLQY in drop-casted film (%)
***n* = 7-10 (MA)**	79.4 ± 0.1	86.8 ± 0.1	70.7 ± 0.1
***n* = 5 (MA)**	68.5 ± 0.1	72.4 ± 1.8	64.7 ± 0.2
***n* = 3 (MA)**	64.8 ± 0.1	68.9 ± 0.1	59.8 ± 0.3
***n* = 1 (MA)**	49.7 ± 0.1	21.7 ± 0.3	13.4 ± 0.1
***n* = 7-10 (FA)**	87.5 ± 0.2	92.5 ± 1.0	72.3 ± 0.1
***n* = 1 (FA)**	60.8 ± 0.4	21.5 ± 0.1	24.8 ± 0.3

Supplementary Movies

movie S1. Ab initio MD of the *n* = 1 geometry viewed along the 001 axis.

movie S2. Ab initio MD of the *n* = 1 geometry viewed along the 100 axis.

movie S3. Ab initio MD of the *n* = 1 geometry viewed along the 010 axis.

Initially the CH_3NH_3 cations are in the [111] configuration and the $PbBr_6$ units form perfect octahedra. Following the first 100 fs the $CH_3NH_3^+$ cations have left their [111] configuration and have assumed many different orientations. It can be seen that there is no coupling between the cations and they are free to move and rotate in space. While the cations move, the negatively charged $PbBr_6^{4-}$ octahedra also distort. This is most likely due to the electrostatic interaction between the two.